Table 1 cell counts for Fig. 1c			
mm from peak	**Total/Max**	**MSE/Max**	**MSE/Total**
Rostral 3.5	10.6 ± 7.1	9.1 ± 5.7	90.9 ± 14.8
Rostral 3.0	16.4 ± 10.6	11.4 ± 8.7	61.5 ± 25.0
Rostral 2.5	15.8 ± 8.2	8.8 ± 6	58.5 ± 29.7
Rostral 2.0	25.9 ± 12.7	13.6 ± 9.5	48.9 ± 20.4
Rostral 1.5	35 ± 17.9	16.5 ± 10	48.8 ± 20.9
Rostral 1	50.1 ± 21.9	23.4 ± 13	50.9 ± 24.4
Rostral 0.5	68.1 ± 20.8	39.5 ± 15.7	58.1 ± 16.8
Peak	89.6 ± 15.7	39.9 ± 17.2	49.0 ± 21.4
Caudal 0.5	72.6 ± 37.5	30.8 ± 19.4	41.2 ± 19.8
Caudal 1.0	29.6 ± 18.3	13 ± 9.1	42.3 ± 25.0
Caudal 1.5	19.1 ± 9.1	6.6 ± 3.4	34.5 ± 6.6

Supplementary Table 1: Specific values for cell counts for premotor spinal neuron distribution.

This table presents the specific values (mean and standard deviation) for the data in Fig. 1c, for the total premotor population and the medial lamina V/VI sub-group, expressed as a fraction of the maximum number of interneurons per cord, per spinal rostro-caudal location. Also presented are the fractions of total premotor neurons found in the medial lamina V/VI cluster at each rostro-caudal location (mean and standard deviation).

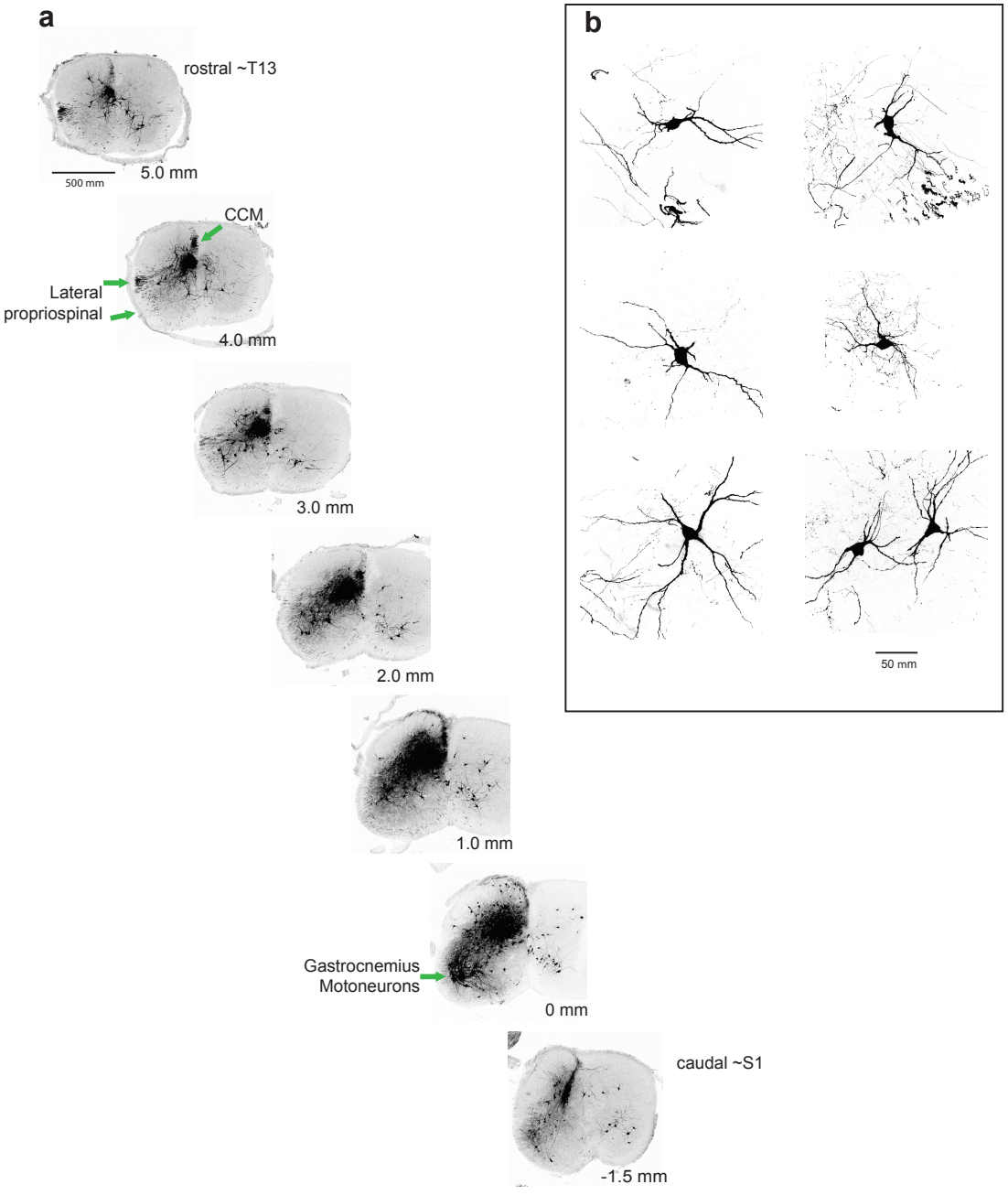

Supplemental Figure 1: Characterization of cellular morphology of MSE column neurons.

(**a**) Transverse 50 μm sections of a spinal cord labeled with RabΔG from the gastrocnemius muscle, showing gastrocnemius motorneurons and pre-gastrocnemius neurons from different rostral (top) to caudal (bottom) levels. The lateral propriospinal white matter tracts and the cornu-commisuralis of Marie (CCM) white matter in the dorsal funiculus are indicated. These white matter tracts are known to contain axons of intersegmentally projecting propriospinal interneurons. MSE column neurons can be seen projecting axons into both white matter tracts. (**b**) Examples of typical cellular morphology of MSE column neurons.

Nature Neuroscience: doi:10.1038/nn.3675

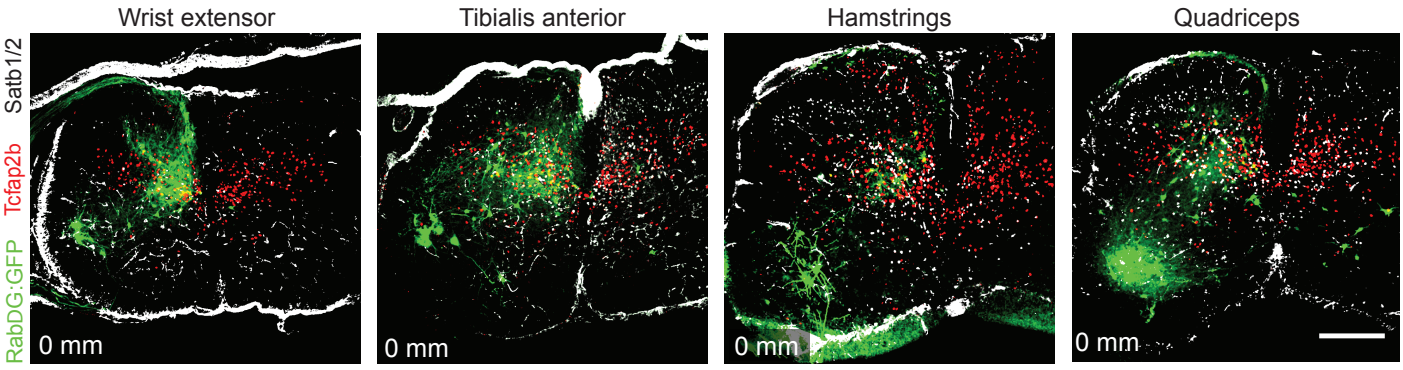

Supplemental Figure 2: Medial deep dorsal horn premotor distribution for diverse muscles.

Distribution of spinal neurons pre-synaptic to the wrist extensor, tibialis anterior, hamstrings, and quadriceps motorneurons, each shown at the level of peak motorneurons for that muscle, together with immunolabeling of Tcfap2β (red) and Satb1/2 (white). Images are projected confocal stacks. Scale bar is 250 μm.

Nature Neuroscience: doi:10.1038/nn.3675

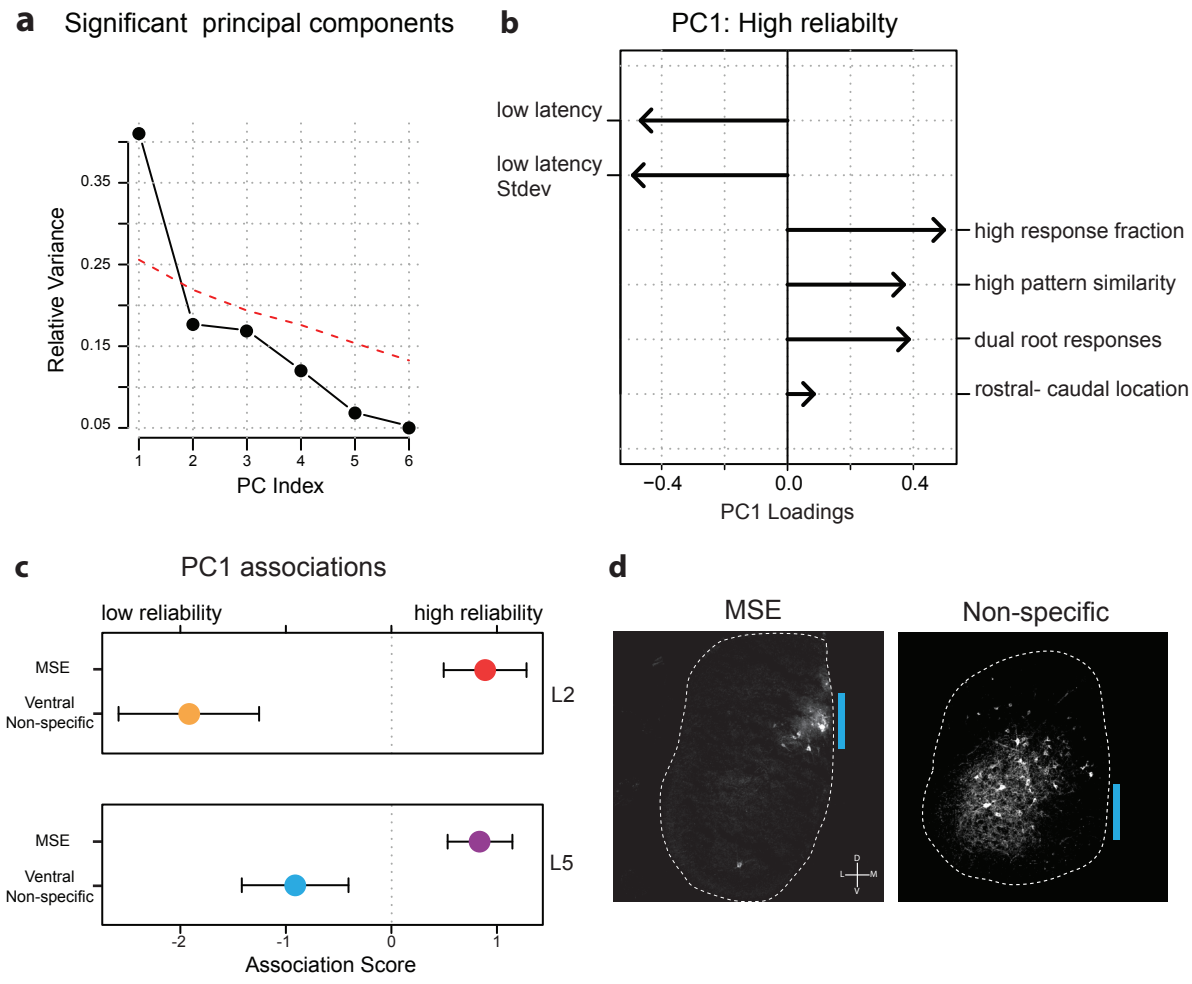

Supplemental Figure 3: Principal component analysis of reliability of evoked motor responses.

(**a**) Principal component significance plot from principal component analysis on the combined data set of MSE and non-specific ventral location summary metrics (see Methods). The first component (PC1) is the only component identified as significant relative to the significance threshold (dashed red line). (**b**) PC1 loading pattern represents a reliability signature of low latency to the first motorneuron spike, low standard deviation in the latency to the first motorneuron spike, a high response fraction among a set of ten trials, high similarity in the pattern of motorneuron spikes, and a high fraction of dual root responses with negligible contribution of rostral-caudal location. (**c**) PC1 association scores (mean and standard error) for MSE evoked L5 (red), MSE evoked L2 (purple), non-specific ventral evoked L5 (orange), and non-specific ventral evoked L2 (blue) responses. A positive association score to PC1 corresponds to greater reliability. (**d**) Examples of hemisected transverse sections for a transynaptic MSE-focused optical stimulation (left) and a non-specific ventral interneuron stimulation (right). The blue bar represents the dorsal-ventral position of light exposure. MSE and intracord experiments had comparable numbers of ChR2-expressing neurons. Transynaptic (MSE) experiments were only considered if the spinal cords met a minimum criteria for efficiency (at least 15 interneurons in a single peak 50 μm section), and the range was 15-30 interneurons in a peak section in the transynaptic ChR2 experiments. In comparison, intracord injections had an average of 35 ± 10 interneuron per section.

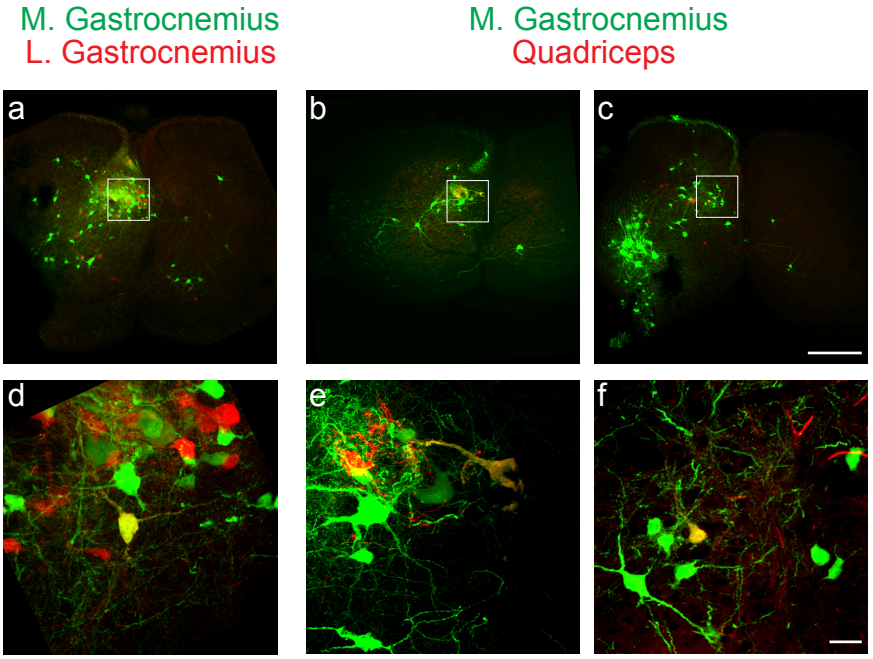

Supplemental Figure 4: MSE neurons target functionally related motor pools.

Individual MSE neurons that directly contact two motor pools were identified using RabΔG:GFP that was injected into the medial gastrocnemius and RabΔG:Cherry was injected into the lateral gastrocnemius or quadriceps at P0. Spinal cords were analyzed at P8. The locations (**a**-**c**) and high magnification views (**d**-**f**) of individual cells that were directly pre-synaptic to the medial gastrocnemius muscle (green) and either the lateral gastrocnemius (red) (**a**,**d**) or the quadriceps (red) (**b**,**c**,**e**,**f**) are shown, as projected confocal images. Double pre-motor MSE are yellow. We found that 13/389 (n=6 cords) pre-medial gastrocnemius neurons were yellow following lateral gastrocnemius or quadriceps injections. We did not observe any yellow cells following injections of the antagonistic pair of medial gastrocnemius and tibialis anterior (0/278), suggesting that yellow double premotor neurons are specifically associated with functionally co-recruited muscles. Scale bars are 250 μm in **a**-**c** and 25 μm in **d**-**f**.

Nature Neuroscience: doi:10.1038/nn.3675

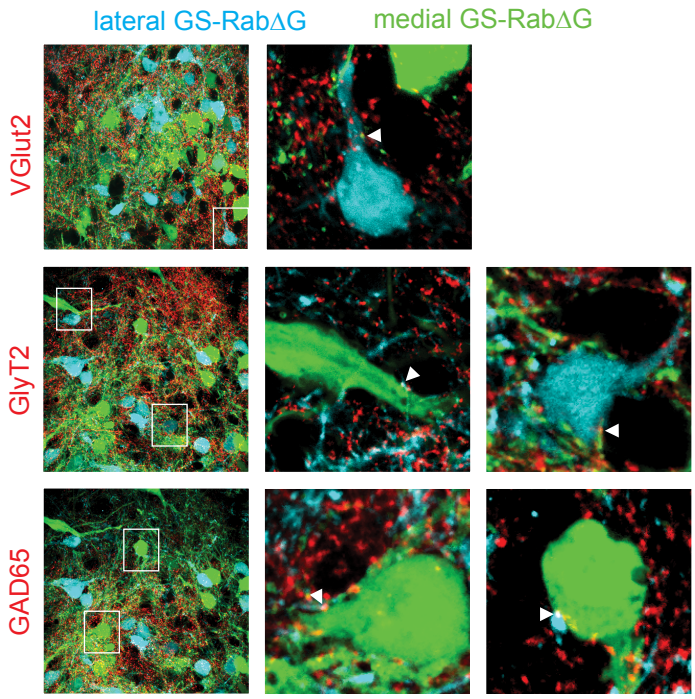

Supplemental Figure 5: Interconnectivity among MSE cells.

Projected confocal images of sections from P8 spinal cords with pre-medial gastrocnemius (medial GS-RabΔG, green) and pre-lateral gastrocnemius (lateral GS-RabΔG, cyan) labeling. Excitatory (vGlut2, red) and inhibitory (Gad65 or GlyT2, red) synaptic contacts between medial GS MSE and lateral GS MSE neurons are highlighted with arrowheads. Middle and right panels are single optical sections.

Nature Neuroscience: doi:10.1038/nn.3675

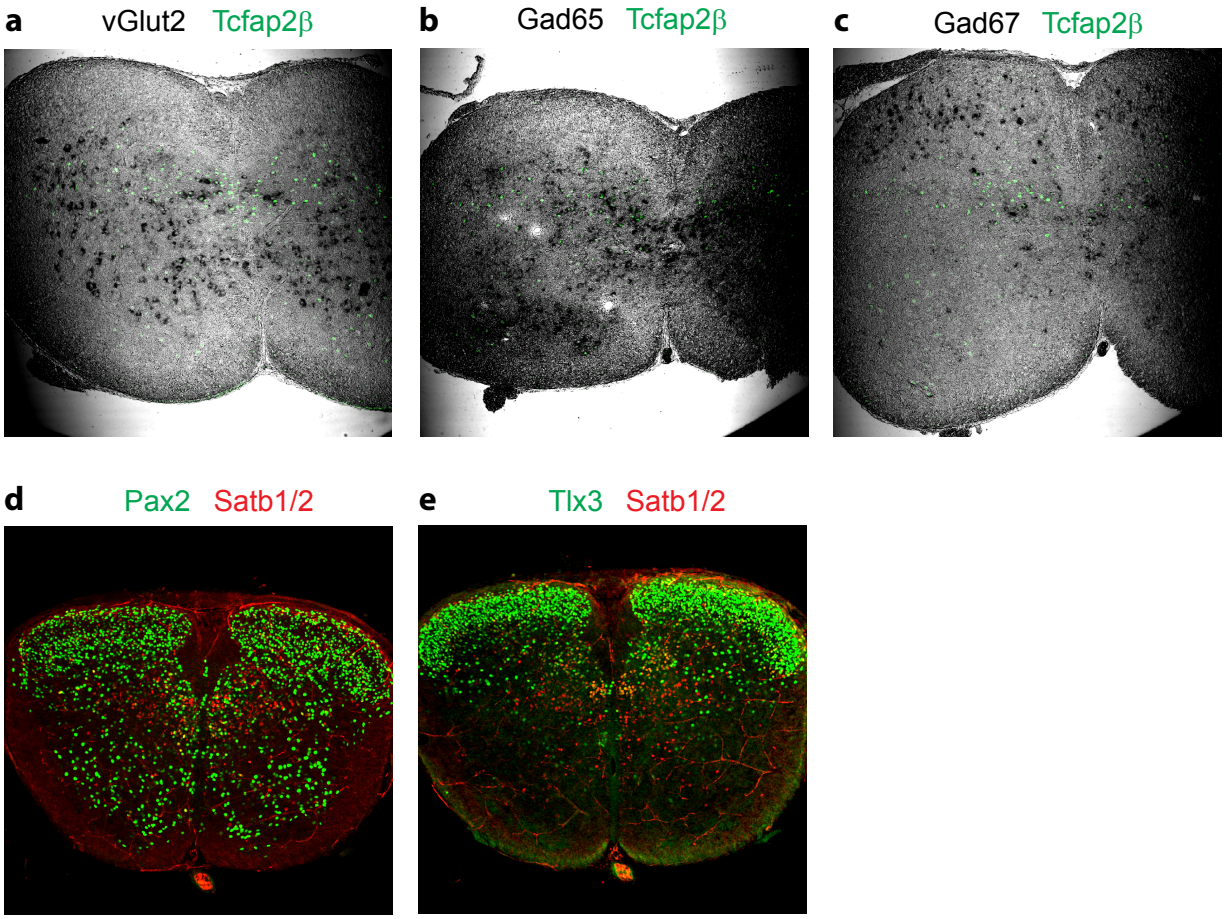

Supplemental Figure 6: Heterogeneity of neurotransmitter expression among MSE neurons.

(**a**-**c**) In situ hybridization in P10 spinal cords against excitatory vGlut2 (**a**), inhibitory Gad65 (**b**), and inhibitory Gad67 (**c**) in black, with immunolabeling against Tcfap2β (green). (**d**-**e**) Immunolabeling in P2 spinal cords against Satb1/2 (red), and inhibitory Pax2 (green) or excitatory Tlx3 (green).

Nature Neuroscience: doi:10.1038/nn.3675

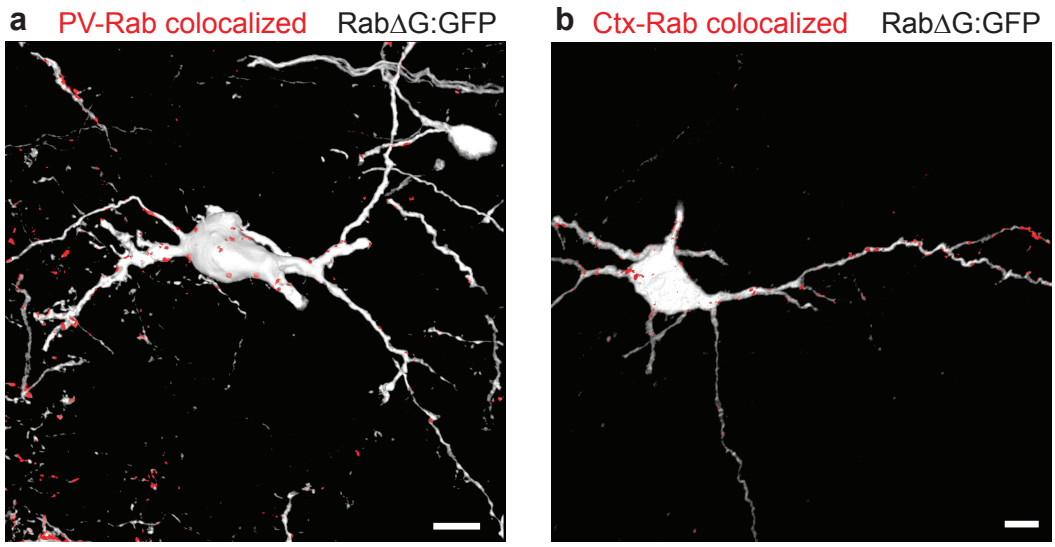

Supplemental Figure 7: Proprioceptive sensory and cortical contacts onto single MSE cells.

(**a**) Three-dimensional reconstruction of proprioceptive (PV-syn-Tomato) colocalized terminals (red) onto a RabΔG labeled pre-gastrocnemius MSE neuron (white). (**b**) Three-dimensional reconstruction of cortical (Ctx-syn-Tomato) colocalized terminals (red) onto a RabΔG labeled pre-TA MSE neuron (white), using Emx1Cre::synaptophysin-tomato. Neurons in a and b express Satb1/2, not shown. Scale bars are 10 μm.

Nature Neuroscience: doi:10.1038/nn.3675

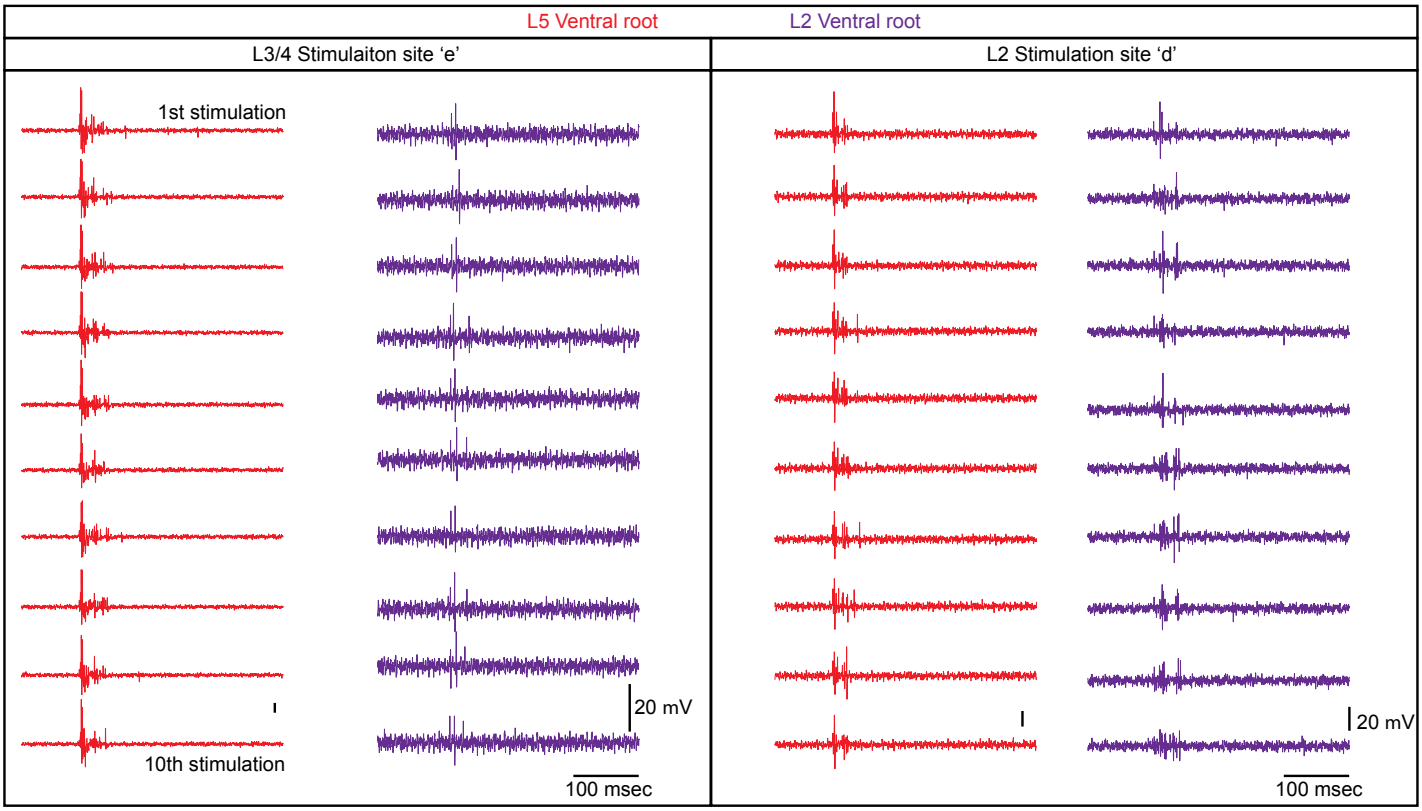

Supplemental Figure 8: Reliability and specificity of distinct motor outputs evoked by optical stimulation of MSE neurons.

L5 (red) and L2 (purple) ventral root responses following 10 trials of optical stimulation of pre-gastrocnemius MSE at L3/L4 (left panel, corresponding to Fig. 6e) and at L2 (right panel, corresponding to Fig. 6d). Note the consistency of the evoked motor patterns. Sets of ten individual traces are shown in each column.

Nature Neuroscience: doi:10.1038/nn.3675

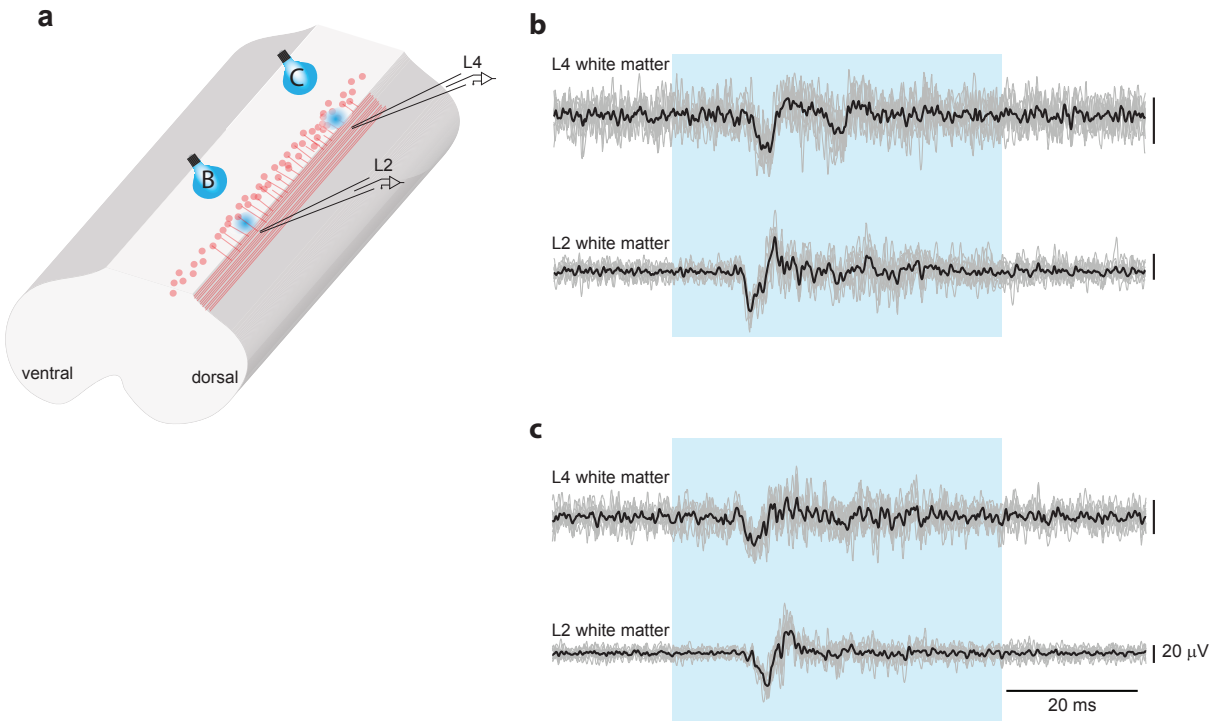

Supplemental Figure 9: Conduction latency within the MSE white matter.

(**a**) Schematic of experimental setup. Electrodes were placed in the cornu-commisuralis of Marie in the deep dorsal funiculus in densities of RabΔ ΔG-labeled MSE axons. (**b**) Optical stimulation at the site of the rostral electrode (L2) evoked spikes in the local white matter (latency 11.6 ms) preceding those at the caudal site by 1.3 ms. Optical stimulation at the caudal site (**c**) reversed this relationship. Electrodes were separated by 1.7 mm. The mean conduction delay in n=4 spinal cords was 0.96 ms/mm.

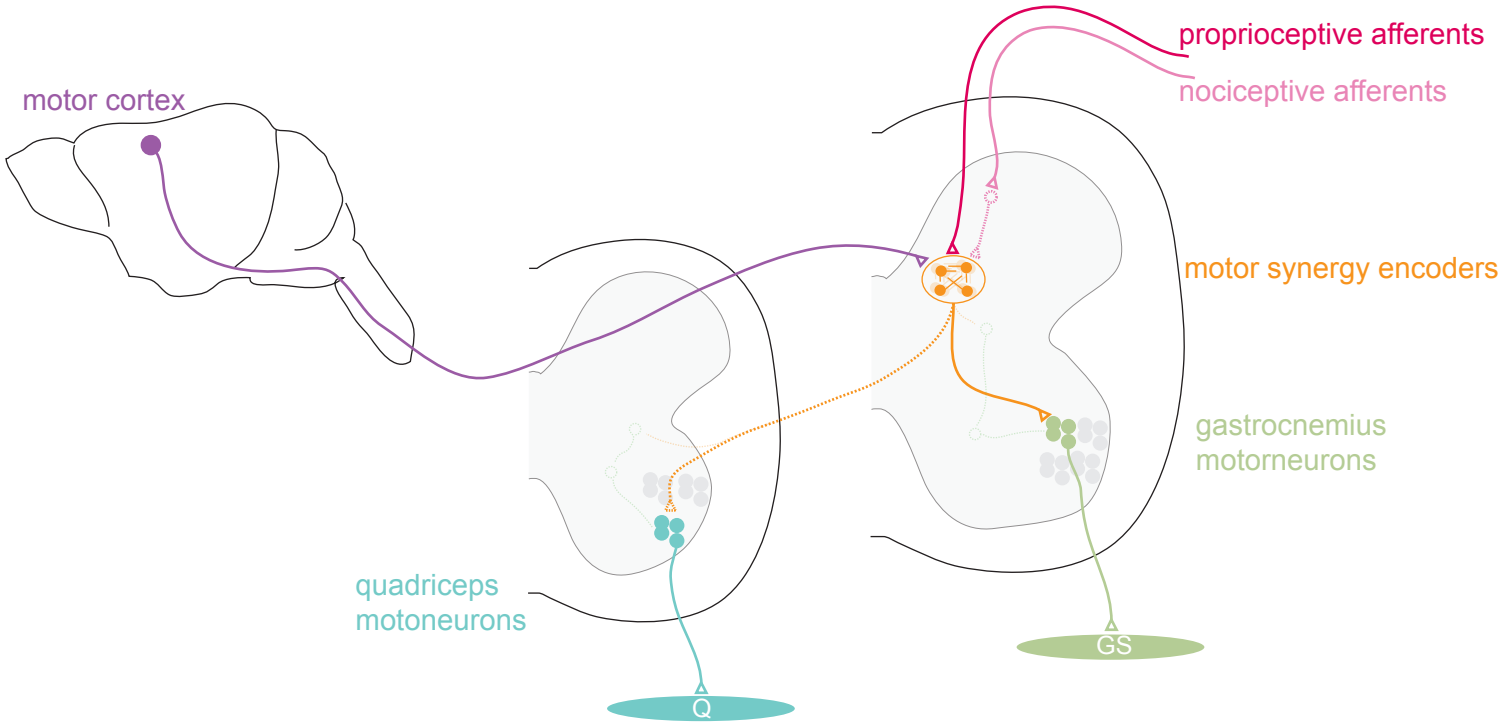

Supplemental Figure 10: MSE cells are a central node in motor control networks.

L2 (left) and L5 (right) lumbar spinal cord segments are depicted with the L5 MSE network (orange). This population receives direct corticospinal (purple) and proprioceptive information (red), and indirect inputs from nociceptive sensory pathways (pink). Outputs include motor pools in multiple segments, such as quadriceps (blue, Q) and gastrocnemius (green, GS).

Nature Neuroscience: doi:10.1038/nn.3675